

The low-frequency properties of FR 0 radio galaxies

A. Capetti¹, R. D. Baldi², M. Brienza^{3,4}, R. Morganti^{5,6}, and G. Giovannini^{3,4}

¹ INAF - Osservatorio Astrofisico di Torino, Strada Osservatorio 20, I-10025 Pino Torinese, Italy

² School of Physics and Astronomy, University of Southampton, Southampton, SO17 1BJ, UK

³ Dipartimento di Fisica e Astronomia, Università di Bologna, Via P. Gobetti 93/2, I-40129, Bologna, Italy

⁴ INAF - Istituto di Radio Astronomia, Via P. Gobetti 101, I-40129 Bologna, Italy

⁵ ASTRON, the Netherlands Institute of Radio Astronomy, Postbus 2, NL-7990 AA, Dwingeloo, the Netherlands

⁶ Kapteyn Astronomical Institute, University of Groningen, PO Box 800, NL-9700 AV Groningen, the Netherlands

ABSTRACT

Using the Alternative Data Release of the TIFR GMRT Sky Survey (TGSS), we studied the low-frequency properties of FR 0 radio galaxies, the large population of compact radio sources associated with red massive early-type galaxies revealed by surveys at 1.4 GHz. We considered TGSS observations from FR0CAT, a sample formed by 104 FR 0s at $z < 0.05$: all but one of them are covered by the TGSS, and 43 of them are detected above a 5σ limit of 17.5 mJy. No extended emission has been detected around the FR 0s, corresponding to a luminosity limit of $\lesssim 4 \times 10^{23} \text{ W Hz}^{-1}$ over an area of $100 \text{ kpc} \times 100 \text{ kpc}$. All but eight FR 0s have a flat or inverted spectral shape ($\alpha < 0.5$) between 150 MHz and 1.4 GHz: this spectral behavior confirms the general paucity of optically thin extended emission within the TGSS beam, as is expected for their compact 1.4 GHz morphology.

Data at 5 GHz were used to build their radio spectra, which are also generally flat at higher frequencies. By focusing on a sub-sample of FR 0s with flux density $> 50 \text{ mJy}$ at 1.4 GHz, we found that $\sim 75\%$ of them have a convex spectrum, but a smaller curvature than the more powerful gigahertz peaked-spectrum sources (GPS). The typical FR 0s radio spectrum is better described by a gradual steepening toward high frequencies, rather than to a transition from an optically-thick to an optically-thin regime, possibly observed in only $\sim 15\%$ of the sample.

Key words. galaxies: active – galaxies: jets

1. Introduction

The identification of the optical counterparts of the large number of sources detected in recent radio surveys at 1.4 GHz (e.g., Best & Heckman 2012) revealed that the majority of the radio sources associated with low redshift galaxies show compact emission, with sizes $\lesssim 10 \text{ kpc}$ (Baldi & Capetti 2009). This population of compact objects was poorly represented in earlier surveys (performed at lower frequency and a higher flux density threshold), which were instead dominated by sources extending over scales of hundreds of kpc (e.g., Hardcastle et al. 1998). Due to the lack of extended radio emission, these “compact” sources were named “FR 0s” (Ghisellini 2011; Sadler et al. 2014; Baldi et al. 2015), a convenient way to include them into the canonical Fanaroff & Riley (1974) classification scheme of radio galaxies (RGs). The information available from observations of FR 0s is generally very limited, even in the radio band. As a consequence, it is still unclear what the nature of these sources is, and how they are related to the other classes of RGs.

Baldi et al. (2018) selected a sample of compact radio sources named FR0CAT, in order to perform a systematic study of FR 0s. FR0CAT consists of 104 compact radio sources with redshift ≤ 0.05 selected by combining observations from the National Radio Astronomy Observatory Very Large Array Sky Survey (NVSS; Condon et al. 1998), the Faint Images of the Radio Sky at Twenty centimeters survey, (FIRST, Becker et al. 1995; Helfand et al. 2015), and Sloan Digital Sky Survey (SDSS; York et al. 2000). In the catalog, Baldi et al. included the sources brighter than 5 mJy and with a limit to the deconvolved angular size of $4''$ in the FIRST images, corresponding to a linear

size $\lesssim 5 \text{ kpc}$. Their radio luminosities at 1.4 GHz are in the $10^{22} \lesssim L_{1.4} \lesssim 10^{24} \text{ W Hz}^{-1}$ range.

Baldi et al. (2019) obtained high-resolution multi-frequency radio images of a sub-sample of 18 FR 0s randomly extracted from FR0CAT. Although the observations reach an angular resolution of $\sim 0''.3$ (corresponding to $\sim 250 \text{ pc}$ at the median redshift of these sources, $z = 0.04$), 14 of the FR 0s are still unresolved, while the remaining four extend over only a few kpc. These observations confirm the general lack of extended radio emission and the high core dominance of FR 0s when compared to the FR 1s of the 3C sample: in FR 1s the fraction of nuclear emission is typically 10^{-2} (Baldi et al. 2019).

The origin of the different nature of FR 0s with respect to the extended RGs still remains to be understood. While the appearance in the radio images of FR 0s and FR 1s is radically different, the nuclear and host galaxies’ properties of these two classes are very similar (Baldi et al. 2018; Torresi et al. 2018). A scenario in which FR 0s are young RGs that will all eventually evolve into extended radio sources cannot be reconciled with the large space density of FR 0s, five times more abundant than FR 1s. FR 0s might instead be recurrent sources, characterized by short phases of activity. Baldi et al. (2015) suggested that the jet properties of FR 0s might be intrinsically different from those of the FR 1s, for example, the former class with lower-bulk Lorentz factors.

In this framework, low-frequency radio observations of FR 0s might play an important role, as they can be used to address the following questions: (1) Do FR 0s show low-frequency extended emission? Compactness is the main defining characteristic of FR 0s and one possibility to account for this property is that they are recurrent sources. In this case, we could

expect to detect remnant emission from a previous cycle of activity. This is typically characterized by a very steep spectrum, and is therefore best observable at MHz-frequencies. (2) What is the low-frequency spectral shape of FR 0s? Observations at high resolution, required to spatially isolate any small-scale extended emission, are only available for a minority of FR 0s. The spectral index information can be used to infer the fraction of optically thin, hence extended, emission present in FR 0s overcoming the limited spatial resolution. (3) What is the fraction of young sources among the FR 0s? Such objects can be found by looking for the characteristic signature of young radio galaxies, meaning, their low-frequency spectral cut-off due to either synchrotron self-absorption (Kellermann 1966; Hodges et al. 1984) or free-free absorption (Kellermann 1966; Bicknell et al. 1997).

The 150 MHz continuum survey performed with the Giant Metrewave Radio Telescope (GMRT; Swarup 1991; Intema et al. 2017) named TGSS (Tata Institute of Fundamental Research GMRT Sky Survey) offers the first possibility to gather low-frequency data with the combination of sensitivity and spatial resolution required for the study of FR 0s. In particular, we will focus on the TGSS observations of the FR0CAT sample.

The paper is organized as follows. In Sect. 2, we list the data available from the TGSS observations of the FR0CAT sources. In Sect. 3, we present our results, which are then discussed in Sect. 4. In Sect. 5, we summarize the results and draw our conclusions.

2. The TGSS data

The low-frequency data for the FR 0s are taken from the TGSS. Intema et al. (2017) produced a first alternative data release (TGSS ADR1) obtained through independent re-processing of the TGSS data. The TGSS ADR1 covers the declination range $-53^\circ < \delta < +90^\circ$ with images at 150 MHz, at a resolution of $\sim 25''$ corresponding to a linear scale between 10 and 25 kpc at the redshift of the sources considered. The median rms noise level of the TGSS ADR1 images is $3.5 \text{ mJy beam}^{-1}$. The catalog contains all sources above the 7σ (24.5 mJy) threshold. The absolute astrometry accuracy of the catalog is better than $2''$.

All but one (namely J0907+35) of the 104 sources of the FR0CAT sample are covered by the TGSS. By adopting a search radius of $5''$, we found an association for 37 out of the 104 FR0CAT sources in the TGSS ADR1 catalog. However, the a priori knowledge of the optical position of the FR 0s enables us to safely use a less stringent limit, which we set at 5σ (17.5 mJy). With this strategy, we recover five additional FR 0 detections. The visual inspection of the TGSS fields of all FR 0 sources also revealed an association for J1559+25, not listed in the catalog, likely because of the presence of a confusing bright (180 mJy at 1.4 GHz) nearby ($29''$) object. We measured a TGSS flux density for J1559+25 of 67.7 mJy. The total number of FR 0s with a 150 MHz flux density measurement is then 43. In Table 1, we list the radio data used for our analysis.

To study the spectral properties of the FR 0s, we also used data from the Green Bank 6-cm survey (GB6, Gregory et al. 1996) and the Westerbork Northern Sky Survey at 327 MHz (WENSS, Rengelink et al. 1997). GB6 covers the Northern sky up to $\delta = 75^\circ$, and it includes the position of all but seven FR0CAT sources. The catalog threshold is generally 18 mJy, but it varies with position within the survey area, being higher at lower declinations (see Tab. 1). The WENSS covers the sky North of $\delta = 30^\circ$, including 25 FR0CAT sources, with a limiting flux density of 18 mJy, and a resolution of $54'' \times 54'' \text{ cosec} \delta$.

Due to the large beams of the TGSS, NVSS, WENSS, and GB6 (with resolutions of $25''$, $45''$, $54''$, and $3'$, respectively), there is the possibility of a contamination from sources located at small distances from the FR0s. We inspected their higher resolution FIRST images to address this issue. Concerning the possible contamination of the first three surveys, we considered an area with a radius of $45''$ (the NVSS beam size) centered on the targeted FR 0: we found that this includes a source present in the FIRST catalog in only two cases: J1427+37 and J1559+25. J1427+37 is not detected at either 150 MHz or 5 GHz. We already identified the confusing source in the TGSS image for J1559+25 (which is not visible in GB6). For these two objects, we used the FIRST flux density value at 1.4 GHz instead of the NVSS value.

To assess any possible contamination of the GB6 measurements, we only considered the 23 FR 0s detected by this survey. For eight of them, there is no FIRST source within $3'$. In 12 cases, the sources within this radius have a flux density at 1.4 GHz between 3% and 10% of the FR 0 considered: even in the case that these sources have an inverted spectrum, they do not produce a significant contribution ($>25\%$) of the measured 5 GHz flux density. In the remaining three cases (namely, J0807+14, J0910+18, and J1111+28), there are nearby sources with flux densities between 30% and 90% of the target of interest. We marked them with an asterisk in Tab. 1 to highlight the possible contamination.

3. Results

The FR 0s detected in the TGSS images (with just one exception) show a single unresolved radio component confirming the lack of large scale extended emission characteristic of these sources seen in both the FIRST and the NVSS. The only exception is J1521+07, also known as 3C 318.1, located at the center of the MKW03S cluster: an extended radio source with an extremely steep spectrum ($\alpha=2.42$ between 235 and 1280 MHz)¹ and a morphology dominated by a peculiar concave arc-like structure (i.e. with its center of curvature located on the opposite side of the J1521+07) is seen ~ 40 kpc toward the south (Giacintucci et al. 2007), a structure possibly not associated with the active nucleus.

We can estimate the limit on the flux density of any extended emission around the FR 0s by considering a fiducial area of $100 \text{ kpc} \times 100 \text{ kpc}$. At the median redshift of the FR0CAT sample of 0.037, this corresponds to $\sim 135'' \times 135''$. The distribution of GMRT antenna baselines is such that the array at 150 MHz is sensitive to extended emission on scales smaller than $68'$ (Intema et al. 2017), much larger than the angular sizes we are interested in. We measured the flux density over $\sim 135'' \times 135''$ in several regions of the FR 0 images. We found a median value of five mJy with a dispersion of 39 mJy, corresponding to a 3σ upper limit of $\sim 120 \text{ mJy}$.

In Fig. 1, we compare the flux densities of the FR0CAT sources at 150 MHz and 1.4 GHz from the TGSS and NVSS, respectively. Since the FR 0s are compact objects, we do not expect the different resolution of the two surveys to significantly affect our results. Conversely, variability is an important issue, particularly because we are dealing with compact sources and considering that ~ 15 years separate the TGSS and NVSS observations. Therefore, the results of this comparison for individual objects should be taken with some caution.

¹ Spectral indices α are defined as $F_\nu \propto \nu^{-\alpha}$.

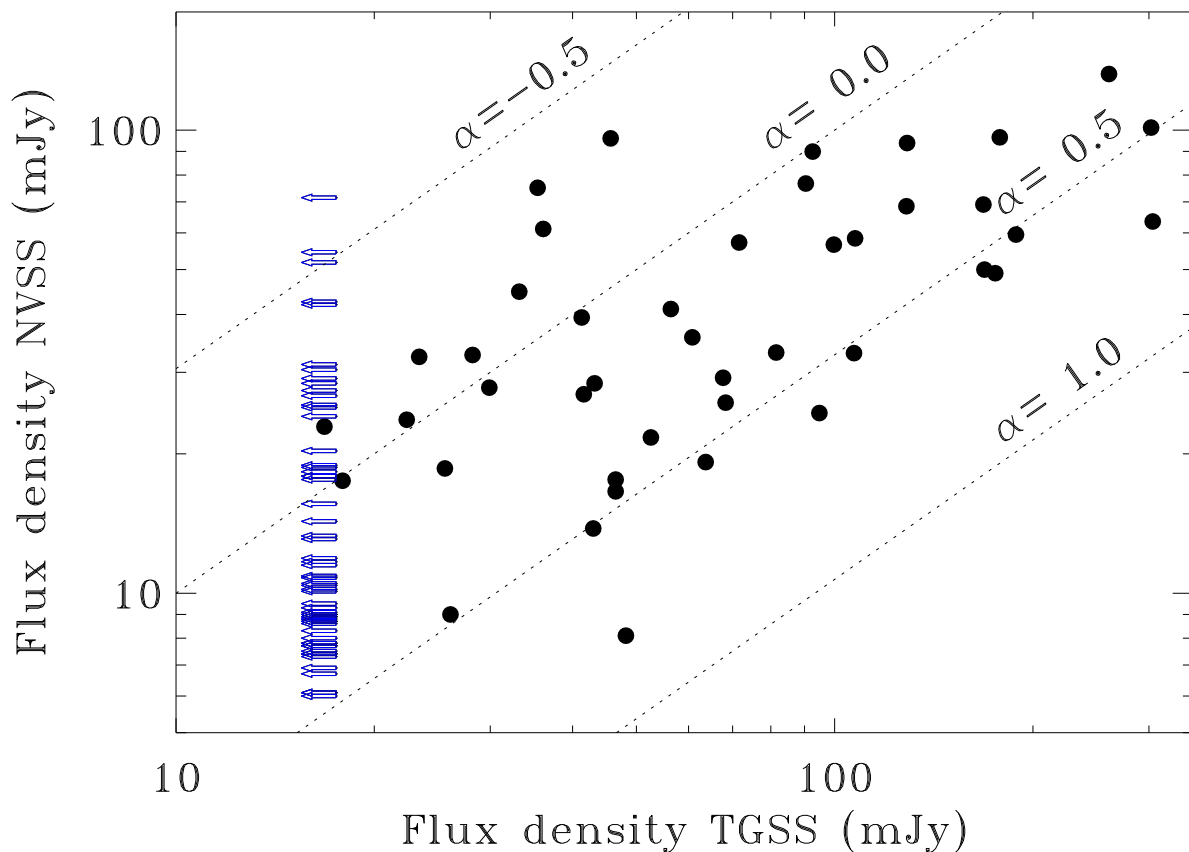


Fig. 1. Comparison of flux densities of FROCAT sources at 150 MHz and 1.4 GHz from TGSS and NVSS, respectively. The dotted lines represent loci of constant spectral indices α (defined as $F_\nu \propto \nu^{-\alpha}$) at the values indicated. The blue, left pointing arrows represent the upper limits in the TGSS.

The resulting spectral indices are steeper than $\alpha > 0.5$ only in eight sources, meaning, the vast majority (92%) of the FR 0s show a flat ($0 < \alpha < 0.5$) or inverted ($\alpha < 0$) low-frequency spectrum. This conclusion applies not only to the sources detected by the TGSS, but also to those with a 150 MHz upper limit, because they all correspond to slopes flatter than $\alpha < 0.47$. Several FR 0s show an inverted spectrum: this is the case of eight of the TGSS detected sources, to which we add the 21 undetected objects with an upper limit $\alpha < 0$ to their spectral indices. The fraction of FR 0s with inverted spectrum is then at least 28%, but it can be as high as 66%, depending on the slope of the remaining 39 FR 0s, undetected in the TGSS, which are all consistent with a negative value of α .

To further investigate the spectral properties of the FR 0s, we also include the GB6 observations at 5 GHz in the analysis and compare the spectral indices measured between 150 MHz and 1.4 GHz, and between 1.4 and 5 GHz (see Fig. 2). This comparison confirms the main conclusion on the paucity of FR 0s with a steep spectrum. The GB6 measurements are also important to finding and to exploring the nature of the sources with a convex spectrum. All sources with $\alpha(150 - 1400) < \alpha(1400 - 5000)$, meaning, those located above the dotted line (marking an equal value of the two spectral indices considered) are objects with a convex spectrum.

A significant limitation of our analysis is related to the relatively small fraction of objects detected at 150 MHz and (or) 5

GHz, due to the higher flux density thresholds of the TGSS and GB6 data with respect to the NVSS. We therefore preferred to restrict this analysis to the sub-sample formed by the 19 FR 0s with a 1.4 GHz flux density $F_{1.4} > 50$ mJy, covered by both the TGSS and GB6 area (see Fig. 2, right panel). At least 14 of these sources have a convex spectrum (see Fig. 3).

Following the approach of O’Dea et al. (1991), we fit the radio spectra with a log-parabola and measured its full width at half maximum (FWHM). We limited our study to the 14 sources with a convex spectrum and measured values typically between 1.5 and six decades (see Fig. 4). The FWHM in five sources must be considered as an upper limit, because the source is not detected in at least one band. The median FWHM is between 2.2 and 2.4 decades, depending on the actual values of the upper limits.

The sampling of the radio spectra of FR 0s is clearly rather limited. For seven of these sources, the spectral coverage can be improved by including the measurements from the WENSS: overall, these support the interpretation that the FR 0s’ spectra are rather shallow. In particular, in two of the sources not detected by the GB6 survey (namely, J1213+50 and J1559+44), the fitted parabolas are consistent with the WENSS data points, suggesting that the upper bounds to their curvature do not differ significantly from their actual values.

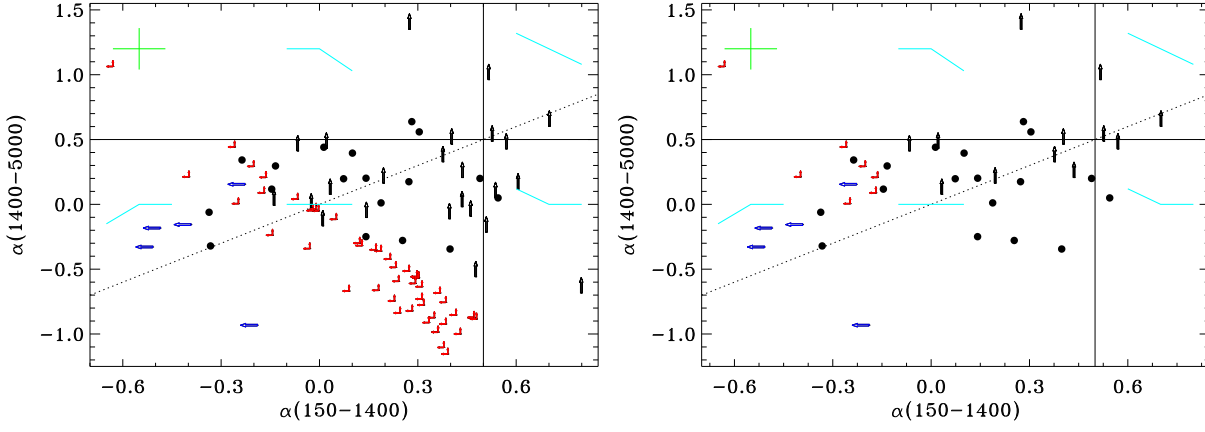


Fig. 2. Left: comparison of spectral indices measured between 150 MHz and 1.4 GHz and 1.4 and 5 GHz. The double red arrows indicate objects only detected at 1.4 GHz, the blue arrows indicate those detected at 1.4 and 5 GHz, but not at 150 MHz, the black arrows indicate those detected at 150 MHz and 1.4 GHz, but not at 5 GHz. The solid lines separate flat ($\alpha < 0.5$) and steep sources. Sources located above the dotted line (marking an equal value of the two spectral indices) are objects with a convex spectrum. The green cross on the upper left corner represents the maximum error, corresponding to the sources with flux density equal to $5 \times \sigma$ in both TGSS and GB6. The cyan broken lines reproduce the typical spectral shape in different regions of the diagram. Right: same as left panel but limited to 19 sources with $F_{1.4} > 50$ mJy.

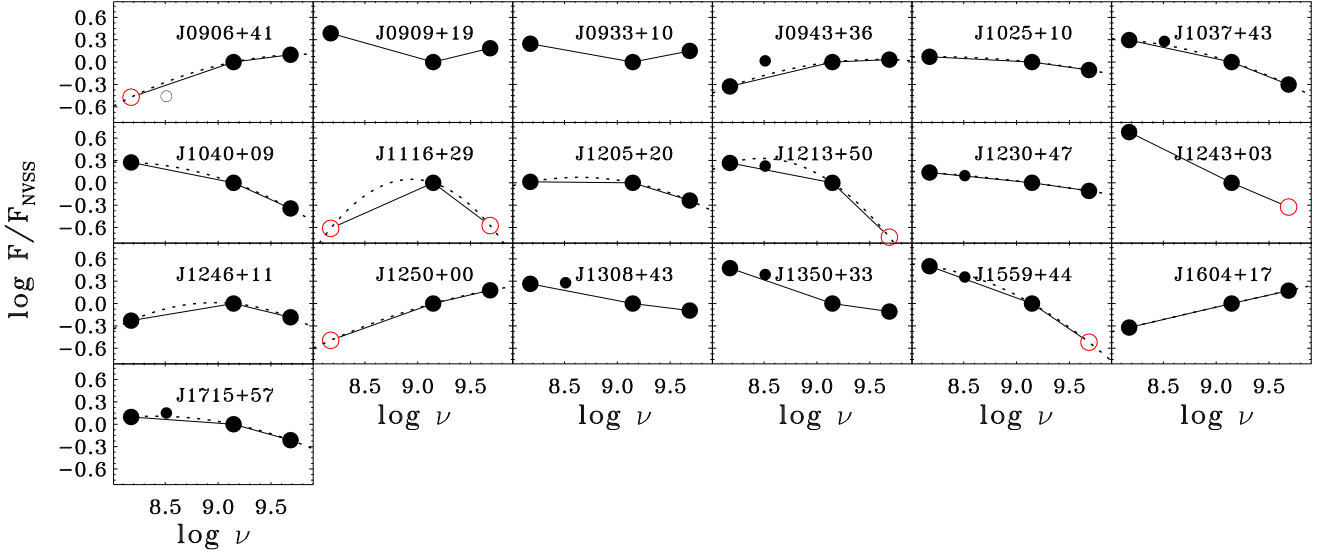


Fig. 3. Radio spectra of the 19 FR 0s with a 1.4 GHz flux density > 50 mJy, covered by both the TGSS and GB6. Flux densities are normalized to unity at 1.4 GHz. The empty red symbols correspond to upper limits. The dashed lines are the log-parabolae defined by the measurements at 150 MHz, 1.4 and 5 GHz which are shown for the sources with a convex spectrum. The smaller symbols are the available WENSS measurements at 327 MHz.

4. Discussion

4.1. Extended radio emission in FR 0s

The TGSS images confirm the lack of spatially extended emission around FR 0s, the main defining property of this class of sources. An extended steep spectrum component might have been expected in two cases. Firstly, FR 0s might be less efficient in the acceleration of the relativistic electrons with respect to standard extended radio-galaxies, and produce intrinsically steep radio spectra. Secondly, FR 0s might be recurrent sources leaving behind a relic emission from previous activity phases, characterized by a steep spectrum due to spectral ageing. The limit to the luminosity of extended structures is $\sim 4 \times 10^{23} \text{ W Hz}^{-1}$ over an area of $100 \text{ kpc} \times 100 \text{ kpc}$ at the median distance of the FR 0 sample. As reference, the edge-darkened FR I sources selected from the same catalog of RGs from which we extracted the FR 0s (Capetti et al. 2017) have sizes between 60 and 120 kpc, and pre-

dicted luminosities at 150 MHz (when assuming a spectral slope of 0.7 between 150 MHz and 1.4 GHz) in the $\sim 10^{24} - 10^{26} \text{ W Hz}^{-1}$ range.

Nonetheless, very low surface brightness emission ($\sim 0.15 \text{ mJy beam}^{-1}$) extending over $\sim 10 \text{ kpc}$ have been detected in NGC 3998 (Frank et al. 2016). NGC 3998 is a nearby ($z=0.0035$) flat-spectrum radio source, unresolved in the FIRST images, fulfilling all requirements for an FR 0 classification.² This individual example indicates that, although FR 0s and FR Is are different classes of sources, deeper observations are needed to explore their relationship in greater depth, and in particular, to establish whether FR 0s are able to produce large-scale jets.

² NGC 3998 is not included in the FR0CAT, because the SDSS did not obtain its optical spectrum.

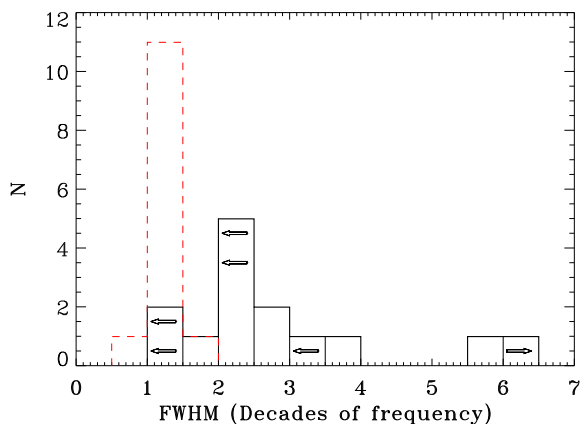


Fig. 4. Black histogram: distribution of FWHM (in decades of frequency) of 14 FR 0s with a convex radio spectrum extracted from 19 sources of bright sub-sample with $F_{1.4} > 50$ mJy. The left pointing arrows correspond to upper limits of the FWHM due to the non detection at least at one frequency. The right pointing arrow represents the FWHM of J1604+17 whose measured value (12.5) exceeds the plot limit. The dashed red histogram reports the FWHM measured by O’Dea et al. (1991) in a sample of 13 GPS.

4.2. Radio spectral properties of FR 0s

The spectral index information can be used to probe the presence of optically-thin emission in FR 0s, and also on scales smaller than the spatial resolution of the TGSS (10 - 25 kpc). The fraction of FR0CAT sources detected by the TGSS is 42%: this relatively low detection rate is due to the combination of (1) the different flux density thresholds used to build the FR0CAT catalog and the one adopted for the TGSS (5 and 17.5 mJy, respectively), and, (2) the generally flat spectral slope between 150 MHz and 1.4 GHz of the FR 0s. Nonetheless, the TGSS sensitivity is sufficient to exclude that the sources not detected by this survey have a spectrum with a slope steeper than 0.5. This leaves us with only eight FR 0s with a steep low-frequency radio spectrum.

A simple model in which the emission is produced by two components, one extended and one compact, with spectral index $\alpha=0.7$ and $\alpha=0$, respectively, indicates that the overall spectrum becomes steep ($\alpha > 0.5$) when the optically-thin component contributes to a fraction $>55\%$ of the total emission at 1.4 GHz. Therefore, at least half the emission from the 35 flat or inverted sources must originate from a core component. This value confirms the high-core dominance of FR 0s derived by Baldi et al. (2019), based on high resolution images.

4.3. Contribution of young radio-galaxies to the FR 0s’ population

A further issue that can be investigated from the low-frequency spectral properties of FR 0s is how many of them are compact because of their youth. Although, as reported in the introduction, the number density of FR 0s is too large to interpret the whole class of compact sources as young objects, the sources that will eventually produce extended RGs must necessarily pass through a small-size phase, and some FR 0s might indeed compact because they are young.

Young RGs can be found looking for a convex spectrum due to a low frequency cut-off. By restricting to the 19 FR 0s with $F_{1.4} > 50$ mJy, the fraction of sources with a convex spectrum is $\sim 75\%$. Nonetheless, the spectral curvature of the FR 0s spectra is less pronounced than what is measured in the more power-

ful GPS sources. O’Dea et al. fit the radio spectra of a sample of GPS with log-parabola (the same method we adopted in the previous section) and found that generally the peak of their radio spectra are rather narrow, with a median value of the FWHM of 1.2 decades of frequency. Conversely, we find larger values, typically between 1.5 and 6 decades (with a median value of ~ 2.3). Although five of them must be considered as upper limits, because the source is not detected in at least one band, the spectral curvature of FR 0s is generally much less pronounced than in GPS.

Apparently, we do not see the sharp transition from an optically-thick to an optically-thin regime typical of the GPS. The spectral properties of FR 0s are better described as being due to a gradual steepening toward high frequencies. Baldi et al. (2019) noted a similar effect in their VLA observations between 1.4 and 7.5 GHz. The spectrum between 4.5 and 7.5 GHz is steeper than between 1.4 and 4.5 GHz, meaning, the high frequency spectra of FR 0s are generally convex: the median difference in the spectral slopes from 1.4 to 5 GHz and from 4.5 to 7.5 GHz is $\Delta\alpha = 0.16$. Baldi et al. also found six out of 18 sources have steep spectra (the remaining objects have flat and, in one case, inverted, spectra), a significantly higher fraction than what we find in this study. Interestingly, the steep sources in the sub-sample³ have a flat spectrum between 150 MHz and 1.4 GHz, confirming the presence of a spectral steepening, with data covering a broader spectral range.

The presence of sources in which the spectral index increases with frequency, similarly to what we see in FR 0s, has been already recognized in very early works and ascribed to the combined effects of self-absorption and of the presence of components with a wide range of brightness temperatures (Kellermann et al. 1969; Marscher 1988). This interpretation might also apply to FR 0s, and it can be tested with radio imaging at a high resolution, sufficient to spatially resolve the various emitting components.

Nonetheless, in the bright sub-sample of 19 FR 0s, there are three sources (namely J0906+41, J1116+29, and J1250+00) whose spectrum is reminiscent of the GPS spectra: they have an inverted spectrum at low-frequencies, and an emission peak at $\nu \gtrsim 1$ GHz. The FR 0s in which we might be observing a genuine low-frequency cut-off, and which can be interpreted as young compact objects, represent $\sim 15\%$ of the sub-sample with flux densities larger than 50 mJy. However, this result must be confirmed with more sensitive surveys. In fact, this flux density limit at 1.4 GHz might introduce a significant bias, because the median luminosity of this sub-sample is a factor 10 higher than for the whole FR0CAT. Furthermore, we might be excluding sources in which the emission peak is located at higher frequencies, and which, for this reason, do not meet the flux density threshold. The very selection of the FR0CAT is based on surveys at 1.4 GHz, and this might represent a bias against sources with a GPS-like spectra.

Furthermore, variability is known to play an important role in the process of identification of this class of sources (see, e.g., Tornaiainen et al. 2005): simultaneous multi-frequency observations are needed to firmly assess their nature. The study of these candidates is particularly relevant because of their extremely low radio luminosity ($2 - 3 \times 10^{23}$ W Hz⁻¹), more than five orders of magnitude below that of the most studied samples of young compact sources (O’Dea 1998), and even less

³ J0907+35, one of the six belonging to this group, is the only FR 0s not covered by the TGSS.

powerful than the low-luminosity compact sources studied by Kunert-Bajraszewska et al. (2010).

5. Summary and conclusions

We present the results obtained from the TGSS survey, based on GMRT observations at 150 MHz of the 104 compact FR 0s sources forming the FR0CAT sample. The fraction of FR 0s detected at low radio frequencies is 36%. The relatively small number of 150 MHz detections is due in part to the higher flux density threshold of the TGSS with respect to the selection threshold of FR0CAT (17.5 and 5 mJy, respectively), but also to the general flatness of the radio spectra: only eight sources have a steep ($\alpha > 0.5$) radio spectral index between 150 MHz and 1.4 GHz.

We failed to detect extended emission associated with the FR 0s. The corresponding upper limit, estimated over a region of $100 \text{ kpc} \times 100 \text{ kpc}$, is $4 \times 10^{23} \text{ W Hz}^{-1}$, a factor between 3 and 300 below the luminosity of FR I sources. In addition, the FR 0s' spectral shapes indicate that the contribution of extended optically-thin emission within the TGSS beam might contribute for, on average, at most a fraction $\lesssim 50\%$ (at 1.4 GHz) to these compact sources.

By also including observations at 5 GHz from the GB6 survey, we explored the radio spectra of FR 0s over a larger range of frequencies. Due to the higher threshold of the GB6 ($\sim 18 \text{ mJy}$), only 23 FR 0s are detected at 5 GHz. We then preferred to limit the multi-band analysis to the sub-sample formed by the 19 FR 0s with a flux density at 1.4 GHz larger than 50 mJy. Most of them (13) have spectral indices flatter than 0.5 in both frequency ranges, and in 14 FR 0s, the spectra is steeper between 1.4 and 5 GHz than between 150 MHz and 1.4 GHz, meaning they are convex spectra.

A convex spectrum is a characteristic feature of young sources in which a turn-over is observed at low frequencies, due to a high optical depth of either free-free or synchrotron self-absorption. This raised the possibility that at least a fraction of the FR0CAT sources are compact, because they are young radio-galaxies. Nonetheless the spectral curvature of FR 0s is in general smaller than in GPS: in FR 0s, the median FWHM is 2.3 decades of frequency compared to a FWHM of 1.2 measured in GPS. The fraction of FR 0s with a high curvature and a spectrum rising in the GHz spectral region, reminiscent of GPS, is at most three out of 19, meaning $\lesssim 15\%$.

Clearly, the studies of the low-frequency radio properties of FR 0s would greatly benefit from the deeper and higher resolution observations that are being produced by the International Low Frequency Array (LOFAR; van Haarlem et al. 2013). In particular, the LOFAR Two-meter Sky Survey (LoTSS) will eventually cover the entire Northern sky, producing $\sim 5''$ resolution images with a sensitivity of $\sim 0.1 \text{ mJy beam}^{-1}$ at 150 MHz (Shimwell et al. 2017). It should enable us to set stronger limits on, or even allow the detection of, the extended emission, with an improvement of the detection threshold of more than an order of magnitude with respect to the TGSS, and to detect the low-frequency counterpart of all the FR 0s with $\alpha(150 - 1400) > -1$. This will enable us to characterize the spectral shape of FR 0s in much greater detail, in particular for those with a convex spectrum.

Acknowledgements. MB acknowledges support from INAF under PRIN SKA/CTA FORECaST and from the ERC-Stg DRANOEL, no 714245. RDB has received funding from the European Union's Horizon 2020 research and innovation programme under grant agreement No 730562 [RadioNet]. TOPCAT astronomical software (Taylor 2005) was used for the preparation and manipulation of the tabular data and the images. We thank the staff of the GMRT that

made these observations possible. GMRT is run by the National Centre for Radio Astrophysics of the Tata Institute of Fundamental Research. This research has made use of Aladin sky atlas developed at CDS, Strasbourg Observatory, France.

References

- Baldi, R. D. & Capetti, A. 2009, *A&A*, 508, 603
 Baldi, R. D., Capetti, A., & Giovannini, G. 2015, *A&A*, 576, A38
 Baldi, R. D., Capetti, A., & Giovannini, G. 2019, *MNRAS*, 482, 2294
 Baldi, R. D., Capetti, A., & Massaro, F. 2018, *A&A*, 609, A1
 Becker, R. H., White, R. L., & Helfand, D. J. 1995, *ApJ*, 450, 559
 Best, P. N. & Heckman, T. M. 2012, *MNRAS*, 421, 1569
 Bicknell, G. V., Dopita, M. A., & O'Dea, C. P. O. 1997, *ApJ*, 485, 112
 Capetti, A., Massaro, F., & Baldi, R. D. 2017, *A&A*, 598, A49
 Condon, J. J., Cotton, W. D., Greisen, E. W., et al. 1998, *AJ*, 115, 1693
 Fanaroff, B. L. & Riley, J. M. 1974, *MNRAS*, 167, 31P
 Frank, B. S., Morganti, R., Oosterloo, T., Nyland, K., & Serra, P. 2016, *A&A*, 592, A94
 Ghisellini, G. 2011, in *American Institute of Physics Conference Series*, Vol. 1381, American Institute of Physics Conference Series, ed. F. A. Aharonian, W. Hofmann, & F. M. Rieger, 180–198
 Giacintucci, S., Venturi, T., Murgia, M., et al. 2007, *A&A*, 476, 99
 Gregory, P. C., Scott, W. K., Douglas, K., & Condon, J. J. 1996, *ApJS*, 103, 427
 Hardcastle, M. J., Alexander, P., Pooley, G. G., & Riley, J. M. 1998, *MNRAS*, 296, 445
 Helfand, D. J., White, R. L., & Becker, R. H. 2015, *ApJ*, 801, 26
 Hodges, M. W., Mutel, R. L., & Phillips, R. B. 1984, *AJ*, 89, 1327
 Intema, H. T., Jagannathan, P., Mooley, K. P., & Frail, D. A. 2017, *A&A*, 598, A78
 Kellermann, K. I. 1966, *Australian Journal of Physics*, 19, 577
 Kellermann, K. I., Pauliny-Toth, I. I. K., & Williams, P. J. S. 1969, *ApJ*, 157, 1
 Kunert-Bajraszewska, M., Gawroński, M. P., Labiano, A., & Siemiginowska, A. 2010, *MNRAS*, 408, 2261
 Marscher, A. P. 1988, *ApJ*, 334, 552
 O'Dea, C. P. 1998, *PASP*, 110, 493
 O'Dea, C. P., Baum, S. A., & Stanghellini, C. 1991, *ApJ*, 380, 66
 Rengelink, R. B., Tang, Y., de Bruyn, A. G., et al. 1997, *A&AS*, 124
 Sadler, E. M., Ekers, R. D., Mahony, E. K., Mauch, T., & Murphy, T. 2014, *MNRAS*, 438, 796
 Shimwell, T. W. & Röttgering, H. J. A., Best, P. N., Williams, W. L., et al. 2017, *A&A*, 598, A104
 Swarup, G. 1991, in *Astronomical Society of the Pacific Conference Series*, Vol. 19, IAU Colloq. 131: Radio Interferometry. Theory, Techniques, and Applications, ed. T. J. Cornwell & R. A. Perley, 376–380
 Taylor, M. B. 2005, in *Astronomical Society of the Pacific Conference Series*, Vol. 347, *Astronomical Data Analysis Software and Systems XIV*, ed. P. Shopbell, M. Britton, & R. Ebert, 29
 Tornaiainen, I., Tornikoski, M., Teräsranta, H., Aller, M. F., & Aller, H. D. 2005, *A&A*, 435, 839
 Torresi, E., Grandi, P., Capetti, A., Baldi, R. D., & Giovannini, G. 2018, *MNRAS*, 476, 5535
 van Haarlem, M. P., Wise, M. W., Gunst, A. W., et al. 2013, *A&A*, 556, A2
 York, D. G., Adelman, J., Anderson, Jr., J. E., et al. 2000, *AJ*, 120, 1579

Table 1. Radio properties of the sample

SDSS name	F(150)	F(1.4)	F(5)	α_1	α_2	SDSS name	F(150)	F(1.4)	F(5)	α_1	α_2
010852.48–003919.4	—	10.9	—	< 0.22	—	123011.85+470022.7	128.8	93.8	73	0.14	0.20
011204.61–001442.4	—	17.9	—	< 0.00	—	124318.73+033300.6	304.0	63.5	<30	0.70	> 0.60
011515.78+001248.4	—	42.6	<33	<-0.40	> 0.21	124633.75+115347.8	36.1	61.2	40	-0.24	0.34
015127.10–083019.3	60.8	35.7	—	0.23	—	125027.42+001345.6	—	54.5	82	<-0.51	-0.33
020835.81–083754.8	—	28.4	—	<-0.20	—	125409.12–011527.1	—	7.7	—	< 0.37	—
075354.98+130916.5	—	7.4	<23	< 0.39	>-0.92	130404.99+075428.4	—	10.5	<26	< 0.23	>-0.74
080716.58+145703.3	43.2	28.4	28*	0.19	0.01	130837.91+434415.1	107.4	58.4	47	0.27	0.17
083158.49+562052.3	26.1 ^a	9.0	<18	0.48	>-0.56	133042.51+323249.0	—	17.9	<19	<-0.01	>-0.04
083511.98+051829.2	—	10.1	<29	< 0.24	>-0.84	133455.94+134431.7	41.3	39.4	<23	0.02	> 0.43
084102.73+595610.5	—	8.9	<18	< 0.30	>-0.57	133621.18+031951.0	—	30.4	<30	<-0.25	> 0.01
084701.88+100106.6	22.4 ^a	23.7	<25	-0.03	>-0.04	133737.49+155820.0	41.6	26.9	<22	0.20	> 0.16
090652.79+412429.7	—	51.8	65	<-0.49	-0.18	134159.72+294653.5	—	10.4	<19	< 0.23	>-0.49
090734.91+325722.9	no data	46.9	<19	—	>-0.76	135036.01+334217.3	302.3	101.3	79	0.49	0.20
090937.44+192808.2	168.2	69.1	106	0.40	-0.34	135226.71+140528.5	—	25.5	<23	<-0.17	> 0.09
091039.92+184147.6	168.8	50.0	47*	0.54	0.05	140528.32+304602.0	—	7.4	<19	< 0.39	>-0.76
091601.78+173523.3	94.8	24.5	<21	0.61	> 0.12	141451.35+030751.2	—	26.7	85	<-0.19	-0.93
091754.25+133145.5	16.8	22.9	<23	-0.14	>-0.01	141517.98–022641.0	—	18.9	—	—	>-0.02
093003.56+341325.3	81.5	33.1	<19	0.40	> 0.46	142724.23+372817.0	—	10.8 ^b	<18	< 0.22	>-0.42
093346.08+100909.0	99.7	56.6	80	0.25	-0.28	143156.59+164615.4	—	8.7	<21	< 0.31	>-0.73
093938.62+385358.6	—	6.1	<18	< 0.47	>-0.88	143312.96+525747.3	—	15.6	<18	< 0.05	>-0.12
094319.15+361452.1	35.4	75.1	81	-0.34	-0.06	143424.79+024756.2	—	7.3	<31	< 0.39	>-1.15
100549.83+003800.0	—	24.1	<32	<-0.14	>-0.24	143620.38+051951.5	—	18.7	<29	<-0.03	>-0.34
101329.65+075415.6	—	7.8	<26	< 0.36	>-0.98	144745.52+132032.2	—	6.7	<23	< 0.43	>-1.00
101806.67+000559.7	—	14.3	<33	< 0.09	>-0.67	145216.49+121711.5	—	8.0	<24	< 0.35	>-0.87
102403.28+420629.8	—	6.0	<18	< 0.48	>-0.88	145243.25+165413.4	17.9 ^a	17.5	<21	0.01	>-0.17
102511.50+171519.9	—	10.2	<21	< 0.24	>-0.59	145616.20+203120.6	68.3	25.8	<20	0.44	> 0.21
102544.22+102230.4	90.4	76.7	60	0.07	0.20	150152.30+174228.2	18.6 ^a	18.6	<21	0.14	>-0.10
103719.33+433515.3	260.9	132.2	66	0.30	0.56	150425.68+074929.7	—	7.8	<27	< 0.36	>-0.99
103952.47+205049.3	—	6.9	<20	< 0.42	>-0.85	150601.89+084723.2	—	8.3	<26	< 0.33	>-0.91
104028.37+091057.1	128.5	68.5	31	0.28	0.64	150636.57+092618.3	27.8 ^a	27.8	<25	0.03	> 0.08
104403.68+435412.0	23.4	32.4	28	-0.15	0.12	150808.25+265457.6	—	20.3	<19	<-0.07	> 0.04
104811.90+045954.8	175.3	49.1	<29	0.57	> 0.43	152010.94+254319.3	—	18.3	<19	<-0.02	>-0.05
104852.92+480314.8	63.7	19.2	<18	0.54	> 0.05	152151.85+074231.7	—	11.7	<27	< 0.18	>-0.66
105731.16+405646.1	33.2	44.8	31	-0.13	0.30	153016.15+270551.0	—	13.3	<19	< 0.12	>-0.30
111113.18+284147.0	56.4	41.1	56*	0.14	-0.25	154147.28+453321.7	—	8.9	<18	< 0.30	>-0.57
111622.70+291508.2	—	71.5	<19	<-0.63	> 1.06	154426.93+470024.2	46.5	17.6	<18	0.43	>-0.02
111700.10+323550.9	—	17.6	<19	<-0.00	>-0.05	154451.23+433050.6	—	11.5	<18	< 0.19	>-0.36
112029.23+040742.1	—	7.5	<30	< 0.38	>-1.10	155951.61+255626.3	67.7 ^a	29.2 ^b	<19	0.38	> 0.33
112256.47+340641.3	46.5	16.6	<19	0.46	>-0.09	155953.99+444232.4	188.5	59.5	<18	0.52	> 0.96
112625.19+520503.5	—	9.0	<18	< 0.30	>-0.56	160426.51+174431.1	45.7	96.0	143	-0.33	-0.32
112727.52+400409.4	43.0	13.8	<18	0.51	>-0.21	160523.84+143851.6	—	8.6	<23	< 0.32	>-0.78
113449.29+490439.4	107.0	33.0	<18	0.53	> 0.49	160641.83+084436.8	—	9.3	<26	< 0.28	>-0.82
113637.14+510008.5	—	9.0	<18	< 0.30	>-0.56	161238.84+293836.9	—	27.4	<19	<-0.20	> 0.29
114230.94–021505.3	—	8.8	—	< 0.31	—	161256.85+095201.5	52.6	21.7	<25	0.40	>-0.11
114232.84+262919.9	—	42.0	51	<-0.39	-0.16	162146.06+254914.4	—	9.1	<19	< 0.29	>-0.61
114804.60+372638.0	—	29.1	24	<-0.23	0.16	162846.13+252940.9	—	25.2	<19	<-0.16	> 0.21
115531.39+545200.4	—	31.2	<18	<-0.26	> 0.44	162944.98+404841.6	—	7.7	<18	< 0.37	>-0.68
120551.46+203119.0	92.6	89.9	52	0.01	0.44	164925.86+360321.3	—	11.9	<18	< 0.17	>-0.35
120607.81+400902.6	—	9.5	<18	< 0.27	>-0.51	165830.05+252324.9	—	13.1	<19	< 0.13	>-0.32
121329.27+504429.4	178.1	96.5	<18	0.27	> 1.35	170358.49+241039.5	28.2	32.7	<20	-0.07	> 0.41
121951.65+282521.3	—	8.7	<19	< 0.31	>-0.64	171522.97+572440.2	71.6	57.2	35	0.10	0.40
122421.31+600641.2	—	6.1	<18	< 0.47	>-0.87	172215.41+304239.8	48.2	8.1	<19	0.80	>-0.68

Column description: (1) name; (2 - 4) flux densities (in mJy) at 0.15, 1.4, and 5 GHz, respectively. (5 - 6) spectral indices between 0.15 and 1.4 GHz (α_1) and 1.4 and 5 GHz (α_2). The sources marked with ^a are those not present in the TGSS catalog, and whose flux density was measured from the images, while those marked with “—” are not detected at 150 MHz with a threshold of 17.5 mJy. For the sources marked with ^b, we used the FIRST measurement instead of the NVSS one, due to the contamination of a nearby source. Sources outside the GB6 survey coverage are indicated with “—” in the last column, while the three FR 0s whose five GHz measurements are potentially contaminated by nearby sources are marked with an asterisk.